An Analytical Solution for Multi-revolution Transfer Trajectory with Periodic Thrust and Non-Singular Elements

By Yusuke OZAWA[1)]

[1)]*Department of Advanced Energy, The University of Tokyo, Kashiwa, Japan*

(Received June 21st, 2017)

Transfer trajectories from low to high altitude orbits include many revolutions, thus take longer, with low-thrust propulsion systems. Propagating this dynamics with planetary equations by full numerical method has a substantial computational cost because of dividing one revolution into tiny arcs of integration. To reduce computational cost, analytical formulae have been developed previously by many researchers. However, these formulae are restricted to particular cases or low-flexibility thrust control models. In order to achieve the desired flexibility, thrust control can be assumed as Fourier series, whose period synchronizes with one orbit period. Additionally, by averaging it over the course of one revolution, high-frequency terms were found to be reduced to a finite number of coefficients of low-frequency terms by the orthogonality condition. This provides a powerful method to reduce computational cost while bring flexibility for thrust control. However, uncertainties occur when a trajectory is close to a circular orbit and/or inclined by a certain angle. This research offers a new analytical solution to overcome above-mentioned issue by employing the equinoctial elements. This new analytical approach then chases only secular variations of exact solutions, thus can be extended to nearly circular orbit cases.

Key Words: Multi-revolutions, Averaging method, Equinoctial Elements, Analytical solution, Low-Thrust propulsion system

Nomenclature

μ	:	standard gravitational parameter for earth 398600 km s^{-2}
a	:	semi-major axis, km
e	:	eccentricity
i	:	inclination, deg
Ω	:	right ascension of ascending node, deg
ω	:	the argument of periapsis, deg
θ	:	the argument of latitude, deg
$\tilde{\omega}$	:	the longitude of periapsis, $\omega + \Omega$, deg
P_1	:	equinoctial element for e, $e \sin \tilde{\omega}$
P_2	:	equinoctial element for e, $e \cos \tilde{\omega}$
Q_1	:	equinoctial element for i, $\tan i/2 \sin \Omega$
Q_2	:	equinoctial element for i, $\tan i/2 \cos \Omega$
M	:	mean anomaly, deg
f	:	true anomaly, deg
E	:	eccentric anomaly, deg
l	:	mean longitude, $M + \tilde{\omega}$, deg
L	:	true longitude, $f + \tilde{\omega}$, deg
K	:	eccentric longitude, $E + \tilde{\omega}$, deg
b	:	semi-minor axis, km
h	:	angular momentum, km^{2}s^{-1}
p	:	semi-latus rectum, km
n	:	mean motion, s^{-1}
T	:	period, s
r	:	radius, km
A	:	thrust acceleration, km s^{-2}
æ	:	equinoctial elements $[a, l, P_1, P_2, Q_1, Q_2]$
$\boldsymbol{x}$	:	Keplerian elements $[a, e, i, \Omega, \omega, M]$
$\boldsymbol{s}$	:	state vector $[r_x, r_y, r_z, v_x, v_y, v_z]$
α	:	cos coefficient of thrust Fourier
β	:	sin coefficient of thrust Fourier

Subscripts

i	:	initial
f	:	final
R	:	radial component
S	:	circumferential component
W	:	normal component

1. Introduction

When a spacecraft using a low-thrust propulsion system escapes from a central body, the trajectory rotates up around the body and the shape becomes spiraling. Designing many-revolution orbit, in which acceleration continuously varies, is computationally expensive, because each integration step has to solve equations of motion which are represented by differential equations with varying thrust profile. Many studies have tackled to reduce the computational cost and analytical solutions have been developed in many special cases, such as a low-eccentricity spiraling model. However, a general design methodology which can solve various many-revolution have never been developed.

Being adapted to general orbit variance, a design method employing perturbation theory have been studied.[1–3)] A spacecraft using low-thrust propulsion have been treated as perturbed Keplerian motion. Approximating it with first order perturbation expansion on one revolution, and formulating analytical solutions, we can eventually know secular variations with low computational cost. However these methods model manoeuvring pattern as constant control for each circles. In other approach, averaged time rate solutions have been found analytically by treating electric thrust profile as a periodic function with Fourier series. This periodical maneuvering, which is included in variational equations of classical orbit elements, could be reduced to finite Fourier coefficients by using trigonometric orthogonality conditions,[4)] i.e. Thrust Fourier Coefficients (TFCs). The Gaussian form Lagrange planetary equations with TFCs are integrated over many-revolution with considerably low computational time and can chase secular variations of a transfer. This analytical method gives high thrust flexibility to trajectory design, and effectively finds out trajectory revolutions by reducing short-term variance. However, this method cannot be used for all cases; e.g. dynamical changing inclination angle, which changes inclination to near zero, or transfering from LEO to GEO and from GTO to GEO, where eccentricity is close to zero. These trajectories are frequently designed for maneuvering around the Earth, however the periapsis points and the line of ascending node are indefinite. In other words, argument of periapsis, right ascension of ascending node and arbitrary anomalies become mathematically undefined value.

In this paper, the above singularity is eliminated by using new orbital elements called equinoctial elements which have non-singularity on zero eccentricity and inclination.[5)] The planetary equations with equinoctial elements are averaged via TFCs theory. Some case studies in this paper prove that this method is suitable to design low eccentricity revolutions with fast computation. The combination of this method and original TFCs theory, which uses Keplerian elements, provides flexibility of maneuvering and transferring for many-revolution.

2. Formulation of Many-Revolutions

2.1. Planetary Equations of Gauss' form

An acceleration of a low-thrust propulsion system is sufficiently small compared to the central gravitational acceleration. Assuming the direction and magnitude of thrust acceleration can be changed continuously, the following Newtonian equation is adequate for describing the dynamics.

$$\dot{\boldsymbol{r}} = \boldsymbol{v} \tag{1}$$

$$\dot{\boldsymbol{v}} = -\frac{\mu}{\boldsymbol{r}^3}\boldsymbol{r} + \boldsymbol{A_d} \tag{2}$$

Time rate of the variational equations formulated by this Newtonian equations are called the Gaussian form of Lagrange planetary equations. The following formula is the definition of accelerating component in RSW (named radial-transverse-normal or satellite coordinate system) reference frame,[6)]

$$\boldsymbol{A_D} = A_R\left(\frac{\boldsymbol{r}}{r}\right) + A_W\left(\frac{\boldsymbol{r}\times\boldsymbol{v}}{|\boldsymbol{r}\times\boldsymbol{v}|}\right) + A_S\left(\frac{\boldsymbol{r}\times\boldsymbol{v}}{|\boldsymbol{r}\times\boldsymbol{v}|}\times\frac{\boldsymbol{r}}{r}\right) \tag{3}$$

One of the expressions for Gaussian planetary equations in RSW frame as below.[5,7)]

$$\frac{da}{dt} = \frac{2a^2}{h}\left(e\sin f A_R + \frac{p}{r}A_S\right) \tag{4}$$

$$\frac{de}{dt} = \frac{1}{h}\left[p\sin f A_R + \{(p+r)\cos f + re\}A_S\right] \tag{5}$$

$$\frac{di}{dt} = \frac{r\cos\theta}{h}A_W \tag{6}$$

$$\frac{d\Omega}{dt} = \frac{r\sin\theta}{h\sin i}A_W \tag{7}$$

$$\frac{d\omega}{dt} = \frac{1}{hf}\{-p\cos f A_R + (p+r)\sin f A_W\} - \frac{r\sin\theta\cos i}{h\sin i}A_W \tag{8}$$

$$\frac{dM}{dt} = n + \frac{b}{ahe}\{(p\cos f - 2re)A_R - (p+r)\sin f A_W\} \tag{9}$$

Integrating these differential equations with any numerical methods, a detailed time history of osculating orbit elements can be shown. Note that following Kepler's equations should be solved to obtain the identical osculating true anomaly and assign it for the next step.

$$M = E - e\sin E \tag{10}$$

$$\tan\frac{1}{2}f = \sqrt{\frac{1+e}{1-e}}\tan\frac{1}{2}E \tag{11}$$

The mean anomaly M is the difference of the mean longitude l and the longitude of periapsis $\tilde{\omega}$. The mean anomaly is transformed to new element ε_1 with a change of variable as following.

$$M = \int n dt + \varepsilon_1 - (\Omega + \omega) \tag{12}$$

Then Eq.(9) takes following form.

$$\frac{d\varepsilon_1}{dt} = -2\sqrt{\frac{a}{\mu}}(1 - e\cos E)A_R + (1 - \sqrt{1-e^2})(\dot{\omega} + \dot{\Omega}) + 2\sqrt{1-e^2}\sin^2\left(\frac{i}{2}\right)\dot{\Omega} \tag{13}$$

2.2. Application of Periodic Thrust Model

According to Fourier's theorem, any piecewise-smooth function $f(\vartheta)$ with a finite number of jump discontinuities on the interval $(0, \Lambda)$ can be expressed by Fourier series:

$$f(\vartheta) \sim \sum_{k=0}^{\infty}\left[a_k\cos\left(\frac{2\pi k\vartheta}{\Lambda}\right) + b_k\sin\left(\frac{2\pi k\vartheta}{\Lambda}\right)\right] \tag{14}$$

When jump discontinuities exist, Fourier series converge to the mean of the two limits. For an interval $\Lambda = m\pi$, the Fourier coefficients are found by

$$a_0 = \frac{1}{m\pi}\int_0^{m\pi} f(\vartheta)d\vartheta \tag{15}$$

$$a_k = \frac{2}{m\pi}\int_0^{m\pi} f(\vartheta)\cos\left(\frac{2k\vartheta}{m}\right)d\vartheta \tag{16}$$

$$b_k = \frac{2}{m\pi}\int_0^{m\pi} f(\vartheta)\sin\left(\frac{2k\vartheta}{m}\right)d\vartheta \tag{17}$$

For any given acceleration component A_D, each component can then be represented as Fourier series over an arbitrary interval. The Fourier series can be expanded in a time-varying orbital parameter, such as f, E, M for ϑ.

$$A_D = \sum_{k=0}^{\infty}\left(\alpha_k^D\cos k\vartheta + \beta_k^D\sin k\vartheta\right) \quad D = R, S, W \tag{18}$$

Thrust curve of each component, that are represented as Fourier series, are substituted to Gaussian planetary equations. Eqs.(4)-(9)

2.3. Averaging method

Averaging the alternation of an open circuit, total amount of variation for one revolution is solved without calculating sequential change. The orbital elements except for anomaly changes slowly for one revolution. Therefore, these elements can be considered as constant parameter in the averaging process.

$$\bar{\dot{x}} = \frac{1}{2\pi}\int_0^{2\pi} \dot{x} dM = \frac{1}{2\pi}\int_0^{2\pi} (1 - e\cos E)\dot{x} dE \tag{19}$$

It is notable that this integration takes a processable form owing to the permutation from mean anomaly to eccentric one because the denominator $(1 + e\cos f)^k$ emerges in the integration process. Some pairs of trigonometric functions appear in the right hand side integrands. Almost orders can be eliminated by the trigonometric orthogonality condition as follows.

$$\int_0^{\Lambda} \cos n\vartheta \cos m\vartheta d\vartheta = \begin{cases} 0 & n \neq m \\ \Lambda & n = m = 0 \\ \Lambda/2 & n = m \neq 0 \end{cases} \tag{20}$$

$$\int_0^{\Lambda} \sin n\vartheta \sin m\vartheta d\vartheta = \begin{cases} 0 & n \neq m \\ \Lambda/2 & n = m \neq 0 \end{cases} \tag{21}$$

$$\int_0^{\Lambda} \sin n\vartheta \cos m\vartheta d\vartheta = 0 \quad all \quad cases \tag{22}$$

Using this orthogonality condition, all Fourier coefficients except for 0th, 1st and 2nd order are removed and can take a simpler form of averaged variational equations.[4)]

$$\left\langle \frac{da}{dt} \right\rangle = 2\sqrt{\frac{a^3}{\mu}}\left(\frac{1}{2}e\beta_1^R + \sqrt{1-e^2}\alpha_0^S\right) \tag{23}$$

$$\left\langle \frac{de}{dt} \right\rangle = \sqrt{\frac{a}{\mu}}\sqrt{1-e^2}\left(\frac{1}{2}\sqrt{1-e^2}\beta_1^R + \alpha_1^S - \frac{3}{2}e\alpha_0^S - \frac{1}{4}e\alpha_2^S\right) \tag{24}$$

$$\left\langle \frac{di}{dt} \right\rangle = \sqrt{\frac{a}{\mu}}\frac{1}{\sqrt{1-e^2}}\left\{\frac{1}{2}(1+e^2)\cos\omega\alpha_1^W - \frac{3}{2}e\cos\omega\alpha_0^W - \frac{1}{2}\sqrt{1-e^2}\sin\omega\beta_1^W - \frac{1}{4}e\cos\omega\alpha_2^W + \frac{1}{4}e\sqrt{1-e^2}\sin\omega\beta_2^W\right\} \tag{25}$$

$$\left\langle \frac{d\Omega}{dt} \right\rangle = \sqrt{\frac{a}{\mu}}\frac{1}{\sqrt{1-e^2}}\left\{\frac{1}{2}\sqrt{1-e^2}\cos\omega\beta_1^W \right. \tag{26}$$

$$\left. + \frac{1}{2}(1+e^2)\sin\omega\alpha_1^W - \frac{1}{4}e\sqrt{1-e^2}\cos\omega\beta_2^W - \frac{1}{4}e\sin\omega\alpha_2^W\right\} \tag{27}$$

$$\left\langle \frac{d\omega}{dt} \right\rangle = \sqrt{\frac{a}{\mu}}\frac{1}{e}\left\{-\frac{1}{2}\sqrt{1-e^2}\alpha_1^R + e\sqrt{1-e^2}\alpha_0^R + \frac{1}{2}(2-e^2)\beta_1^S - \frac{1}{4}e\beta_2^S\right\} - \cos i\left\langle\dot{\Omega}\right\rangle \tag{28}$$

$$\left\langle \frac{d\varepsilon_1}{dt} \right\rangle = \sqrt{\frac{a}{\mu}}\left\{(-2-e^2)\alpha_0^R + 2e\alpha_1^R - \frac{1}{2}e^2\alpha_2^R\right\} + \left(1 - \sqrt{1-e^2}\right)\left(\langle\dot{\omega}\rangle + \left\langle\dot{\Omega}\right\rangle\right) + 2\sqrt{1-e^2}\sin^2\frac{i}{2}\left\langle\dot{\Omega}\right\rangle \tag{29}$$

These particular remaining coefficients are called as Thrust Fourier Coefficients (TFCs)[4)] is next presented.

$$\alpha_{0,1,2}^R, \quad \beta_1^R, \quad \alpha_{0,1,2}^S \quad \beta_{1,2}^S, \quad \alpha_{0,1,2}^W \quad \beta_{1,2}^W \tag{30}$$

In this paper, for distinction with TFCs derived from averaging with equinoctial elements, these coefficients are named as KTFCs (Keplerian TFCs).

3. New Formulation with Equinoctial Elements

3.1. Planetary Equations with Equinoctial Elements

Right ascension of ascending node Ω and argument of periapsis ω are defined upon the line of ascending node, hence, when the orbit inclination is close to zero ($i \sim 0$), these values (Ω and ω) become undefined ones due to the undetermined line of ascending node. Furthermore, ω and the anomalies f, M, E are measured from the direction of periapsis, thus as the orbit shape is approaching to a true circle ($e \sim 0$), these values (ω and anomalies f, M, E) become undefined due to the undetermined periapsis. Accordingly, ω, Ω, i, e, and anomalies should be transformed into new elements which have no singularity for above cases. In order to find the non-singular elements, new elements must be defined so as not to depend on the line of ascending node and periapsis.

For instance, adding both Ω and ω, the singularity about the line of ascending node is vanished. The next formulation define the longitude of periapsis $\tilde{\omega}$.

$$\tilde{\omega} \equiv \Omega + \omega \tag{31}$$

Nevertheless, the singularity related to eccentricity e still exists, in other words, there is a singularity related to periapsis, so the longitude of periapsis $\tilde{\omega}$ itself is not a non-singular element. Similarly, adding M to $\tilde{\omega}$, new element is defined as below, and is not singular for both the line of ascending node and periapsis.

$$l \equiv \tilde{\omega} + M \tag{32}$$

The mean anomaly M can be replaced by the mean longitude l, however, it has not yet applied to the uncertainty about true anomaly f (See the original Gaussian planetary equations as shown in Eqs.(4)-(9)). This singularity can be detected by examining Kepler equation thoroughly.

$$l = \tilde{\omega} + M = \tilde{\omega} + E - e\cos E \tag{33}$$

Here, the eccentric longitude is defined so as to correspond to the true longitude,

$$K \equiv \tilde{\omega} + E \tag{34}$$

$$L \equiv \tilde{\omega} + f \tag{35}$$

Then, Kepler's equation is rewritten as following

$$l = K + e\sin\tilde{\omega}\cos K - e\cos\tilde{\omega}\sin K \tag{36}$$

Moreover, the orbit equation could be transformed to the eccentric longitude and the true longitude. According to the definition of the orbit equations.

$$\begin{aligned} r &= a(1 - e\cos E) \\ &= a(1 - e\sin\tilde{\omega}\sin K - e\cos\tilde{\omega}\cos K) \end{aligned} \tag{37}$$

and,

$$r = p/(1 + e\cos f) \\ = p/(1 + e\sin\tilde{\omega}\sin L + e\cos\tilde{\omega}\cos L) \tag{38}$$

Eccentricity e and longitude of periapsis $\tilde{\omega}$ are appeared like $e\sin\tilde{\omega}$ and $e\cos\tilde{\omega}$ on both the orbit equations and Kepler's equation. These terms can be replaced to new elements which avoid the singularity of periapsis in low eccentricity case.

$$P_1 \equiv e\sin\tilde{\omega} \quad \textit{and} \quad P_2 \equiv e\cos\tilde{\omega} \tag{39}$$

Differentiating these new elements with respect to time, by substituting the variational equations for e and $\tilde{\omega}$ as defined in Eq.(5),(7) and (8), the new planetary equations for P_1 is defined as below.

$$\begin{aligned}\frac{dP_1}{dt} &= e\cos\tilde{\omega}\frac{d\tilde{\omega}}{dt} + \sin\tilde{\omega}\frac{de}{dt} \\ &= -\frac{1}{h}\left[p\cos LF_W - (p+r)\sin LA_S\right. \\ &\qquad \left. -rP_1A_W + \frac{r\sin\theta\tan\frac{i}{2}}{h}P_2A_W\right]\end{aligned} \tag{40}$$

In the case of P_2, the same procedure is applied.

And, argument of latitude also needs to be expressed by the true longitude L.

$$\theta = \omega + f = L - \Omega \tag{41}$$

thus,

$$\sin\theta = \sin L\cos\Omega - \cos L\sin\Omega \tag{42}$$

Right ascension of ascending node Ω is not a non-singular element, however, $\sin\theta$ emerges on the product with $\tan(i/2)$. The terms, $\tan(i/2)\cos\Omega$ and $\tan(i/2)\sin\Omega$ becomes the candidates for replacing to new elements.

$$Q_1 \equiv \tan\frac{i}{2}\sin\Omega \quad \textit{and} \quad Q_2 \equiv \tan\frac{i}{2}\cos\Omega \tag{43}$$

Differentiating the new elements by assigning the classical planetary equations as shown in Eq.(6) and (7), the new expression is obtained.

$$\begin{aligned}\frac{dQ_1}{dt} &= \tan\frac{i}{2}\cos\Omega\frac{d\Omega}{dt} + \frac{1}{2}\sec^2\frac{i}{2}\sin\Omega\frac{di}{dt} \\ &= \frac{r}{2h}\sec^2\frac{i}{2}(\sin\theta\cos\Omega + \cos\theta\sin\Omega)A_W \\ &= \frac{r}{2h}(1 + Q_1^2 + Q_2^2)\sin LA_W\end{aligned} \tag{44}$$

The variations of Q_2 is also introduced via the same procedure.

Consequently, the foundation for non-singular elements a, P_1, P_2, Q_1, Q_2, l is established. These elements are defined upon equinoctial plane and the direction of vernal equinox. Hence, these elements are called as equinoctial elements. Besides, the new formulation of Gaussian planetary equations is found in the above process, and there are as below.[5)]

$$\frac{da}{dt} = \frac{2a^2}{h}\left\{(P_2\sin L - P_1\cos L)A_R + \frac{p}{r}A_S\right\} \tag{45}$$

$$\begin{aligned}\frac{dl}{dt} &= n - \frac{r}{h}\left[\left\{\frac{a}{a+b}\left(\frac{p}{r}\right)(P_1\sin L + P_2\cos L) + \frac{2b}{a}\right\}A_R\right. \\ &\quad + \frac{a}{a+b}\left(1 + \frac{p}{r}\right)(P_1\cos L - P_2\sin L)A_S \\ &\quad \left. + (Q_1\cos L - Q_2\sin L)A_W\right]\end{aligned} \tag{46}$$

$$\begin{aligned}\frac{dP_1}{dt} &= \frac{r}{h}\left[-\frac{p}{r}\cos LF_R + \left\{P_1 + \left(1 + \frac{p}{r}\right)\sin L\right\}A_S\right. \\ &\quad \left. -P_2(Q_1\cos L - Q_2\sin L)A_W\right]\end{aligned} \tag{47}$$

$$\begin{aligned}\frac{dP_2}{dt} &= \frac{r}{h}\left[\frac{p}{r}\sin LF_R + \left\{P_2 + \left(1 + \frac{p}{r}\right)\cos L\right\}A_S\right. \\ &\quad \left. +P_1(Q_1\cos L - Q_2\sin L)A_W\right]\end{aligned} \tag{48}$$

$$\frac{dQ_1}{dt} = \frac{r}{2h}(1 + Q_1^2 + Q_2^2)\sin LA_W \tag{49}$$

$$\frac{dQ_2}{dt} = \frac{r}{2h}(1 + Q_1^2 + Q_2^2)\cos LA_W \tag{50}$$

where,

$$b = a\sqrt{1 - P_1^2 - P_2^2} \tag{51}$$

$$h = nab \tag{52}$$

$$\frac{p}{r} = 1 + P_1\sin L + P_2\cos L \tag{53}$$

$$\frac{r}{h} = \frac{h}{\mu(1 + P_1\sin L + P_2\cos L)} \tag{54}$$

For a numerical integration algorithm, to obtain true longitude, we have to solve two transcendental equations in each iteration steps.

$$l = K + P_1\cos K - P_2\sin K \tag{55}$$

$$r = a(1 - P_1\sin K - P_2\cos K) \tag{56}$$

The eccentric longitude K and the radius r are obtained by employing previous equations. Finally, the true longitude L is defined with following relational expressions.

$$\sin L = \frac{a}{r}\left[\left(1 - \frac{a}{a+b}P_2^2\right)\sin K + \frac{a}{a+b}P_1P_2\cos K - P_1\right] \tag{57}$$

$$\cos L = \frac{a}{r}\left[\left(1 - \frac{a}{a+b}P_1^2\right)\cos K + \frac{a}{a+b}P_1P_2\sin K - P_2\right] \tag{58}$$

3.2. Averaging with Eccentric Longitude

To reduce the computational cost, it is appropriate to apply an averaging method to design many-revolution. In the case of Gaussian planetary equations with equinoctial elements, the true longitude L performs as a time-varying parameter. Accordingly, when the planetary equations are averaged with respect to the true longitude, the factor $(1 + P_1\sin L + P_2\cos L)$ remains as denominator in the integrating process.

$$\int_0^{2\pi}\frac{\sin L\left(\sum_{k=0}^{\infty}\alpha_k\cos kL + \beta_k\sin kL\right)}{1 + P_1\sin L + P_2\cos L}dL \tag{59}$$

Solving these integrands numerically, it is found that integral value on the higher order does not converge to zero. For this reason, it is impossible to find an analytical form with the true longitude. The original TFCs theory, which uses classical Keplerian elements, can obtain analytical solutions by replacing to eccentric anomaly E. Similarly, the eccentric longitude can be converted from the true anomaly with the relations given in Eqs.(57)-(58) and the orbital equation Eq.(56). However, the orthogonality of trigonometric functions cannot be used because of the existence of factor $(1 - P_1 \sin K - P_1 \cos K)$ as denominator.

$$\int_0^{2\pi} \frac{\sin K \left(\sum_{k=0}^{\infty} \alpha_k \cos kK + \beta_k \sin kK\right)}{1 - P_1 \sin K - P_2 \cos K} dK \tag{60}$$

This denominator is emerged due to the substitution of relational expressions, which have the term r at denominator. Hence, these terms can be canceled by multiplying r for both sides.

$$r \int_0^{2\pi} \frac{\sin K \left(\sum_{k=0}^{\infty} \alpha_k \cos kK + \beta_k \sin kK\right)}{1 - P_1 \sin K - P_2 \cos K} dK$$
$$= a \int_0^{2\pi} \sin K \left(\sum_{k=0}^{\infty} \alpha_k \cos kK + \beta_k \sin kK\right) dK = a\beta_1 \pi$$

The right hand sides of the variational equations are simplified and can then use the orthogonality conditions. On the other hand, the left hand side is represented as following.

$$\langle r\dot{x} \rangle = \langle r \rangle \langle \dot{x} \rangle + \langle r' \dot{x}' \rangle \tag{61}$$

The 2$^{\text{nd}}$ term on the right hand side shows the averaged product of both the deviation of radius and the variances of elements, which correspond to the covariance for one revolution. When orbit is extremely almost a circle, the deviation of radius r' becomes small so as to be able to ignore the 2$^{\text{nd}}$ term. Consequently, the merit to be able to avoid the singularity problem in low eccentricity is guaranteed.

$$\langle r\dot{x} \rangle \simeq \langle r \rangle \langle \dot{x} \rangle = a \langle \dot{x} \rangle \tag{62}$$

$$\langle r \rangle = \frac{1}{2\pi} \int_0^{2\pi} a(1 - P_1 \sin K - P_2 \cos K) dK = a \tag{63}$$

For instance, the formulation process for a is shown. At first, both sides of the variational equations as in Eq.(45) are multiplied by the radius r, and the previous equations (Eqs.56,57 and 58) are applied to the first and the second term.

$$\begin{aligned} r\frac{da}{dt} &= \frac{2a^2}{h}\left(P_2 r \sin L - P_1 r \cos L\right) F_R \\ &+ \frac{2a^2}{h}\left(r + P_1 r \sin L + P_2 r \cos L\right) F_S \\ &= \frac{2a^3}{h(a+b)}\left(aP_1^2 + aP_2^2 - a - b\right)\left(P_1 \cos K - P_2 \sin K\right) \\ &- \frac{2a^3}{h}\left(P_1^2 + P_2^2 - 1\right) \end{aligned} \tag{64}$$

averaging this,

$$\begin{aligned} \left\langle r\frac{da}{dt} \right\rangle &= \frac{2a^3}{h(a+b)}\left(aP_1^2 + aP_2^2 - a - b\right)\left(P_1 \frac{\alpha_1^R}{2} - P_2 \frac{\beta_1^R}{2}\right) \\ &- \frac{2a^3}{h}\left(P_1^2 + P_2^2 - 1\right)\alpha_0^S \end{aligned} \tag{65}$$

Only the Fourier coefficients of lower orders remain. The left hand side averaged product can be converted to the companion of averages under the construction of low eccentricity (eq.62).

$$\begin{aligned} \left\langle \frac{da}{dt} \right\rangle &= \frac{2a^2}{h(a+b)}\left(aP_1^2 + aP_2^2 - a - b\right)\left(P_1 \frac{\alpha_1^R}{2} - P_2 \frac{\beta_1^R}{2}\right) \\ &- \frac{2a^2}{h}\left(P_1^2 + P_2^2 - 1\right)\alpha_0^S \end{aligned} \tag{66}$$

Then, we obtain the averaged planetary equations for semi-major axis a. For the other elements, the same procedure allows it to be formulated. This averaging process reveals that the averaged mean longitude yields the new Fourier coefficients β_2^R. In this paper, we do not mention that how the coefficients works for the secular variations, yet in spite of that this fact says that, around the singularity, a more detailed thrust model is performed for long-time fluctuations. Note that these remained ones are named as Equinoctial Thrust Fourier Coefficients set (ETFCs) in this paper.

$$\alpha_{0,1,2}^R, \quad \beta_{1,\mathbf{2}}^R, \quad \alpha_{0,1,2}^S \quad \beta_{1,2}^S, \quad \alpha_{0,1,2}^W \quad \beta_{1,2}^W \tag{67}$$

The following is the vectorized form of this averaged planetary equations.

$$\left\langle \frac{d\text{æ}}{dt} \right\rangle = M_R \boldsymbol{f}_{\boldsymbol{R}}^T + M_S \boldsymbol{f}_{\boldsymbol{S}}^T + M_W \boldsymbol{f}_{\boldsymbol{W}}^T \tag{68}$$
$$\boldsymbol{f}_{\boldsymbol{D}} = \begin{bmatrix} \alpha_0^D & \alpha_1^D & \alpha_2^D & \beta_1^D & \beta_2^D \end{bmatrix} \qquad D = \{R, S, W\}$$

M_R, M_S, M_W are the modulus matrices for each ETFCs as shown in Eqs.69,70,71.

3.3. Applying to Integration Algorithm

The appropriate Keplerian elements are decided for the beginning as osculating orbit elements. These elements are converted to the equinoctial elements with the equations as shown in Eqs.(32),(39) and (43). Next, these initial osculating equinoctial elements are determined as the initial condition æ_i, and calculate the variance of this revolution $\langle \dot{\text{æ}} \rangle$ with the algebraic expression as shown in Eq.(68). The period of this revolution is solved with initial osculating semi-major axis. Finally, the final osculating equinoctial elements are propagated like below form.

$$\text{æ}_f = \left\langle \frac{d\text{æ}}{dt} \right\rangle T + \text{æ}_i \tag{72}$$

Each final osculating equinoctial elements are solved similarly for each revolution; thus, the number of revolutions are 10, and the number of solutions are 11. The solutions are linearly interpolated in between. To understand instinctively the variations of many-revolution, equinoctial elements should be convert to Keplerian elements. Keplerian is obtained by these equations.[5)]

$$e^2 = P_1^2 + P_2^2 \tag{73}$$

$$\tan^2 \frac{i}{2} = Q_1^2 + Q_2^2 \tag{74}$$

$$\tan \tilde{\omega} = \frac{P_1}{P_2} \tag{75}$$

$$\tan \Omega = \frac{Q_1}{Q_2} \tag{76}$$

$$
M_R = \begin{bmatrix}
0 & \frac{a^2(\delta\epsilon_1-1)P_1}{h} & 0 & -\frac{a^2(\delta\epsilon_1-1)P_2}{h} & 0 \\
\frac{\delta((h-b)\epsilon_1-2b)}{\mu} & \frac{\delta(4b-h)P_2}{2\mu} & \frac{\delta b\epsilon_2}{2\mu} & \frac{\delta(4b-h)P_1}{2\mu} & -\frac{\delta b\epsilon_5}{2\mu} \\
\frac{hP_2}{\mu} & \frac{h(\delta P_1^2-1)}{2\mu} & 0 & -\frac{ha\epsilon_5}{4\mu} & 0 \\
-\frac{hP_1}{\mu} & \frac{ha\epsilon_5}{4\mu} & 0 & \frac{h(1-\delta P_2^2)}{2\mu} & 0 \\
0 & 0 & 0 & 0 & 0 \\
0 & 0 & 0 & 0 & 0
\end{bmatrix} \tag{69}
$$

$$
M_W = \begin{bmatrix}
0 & 0 & 0 & 0 & 0 \\
-\lambda_4 & \frac{\delta P_1\lambda_1-Q_1}{2} & 0 & -\frac{\delta P_2\lambda_1-Q_2}{2} & 0 \\
-\frac{3aP_2\lambda_4}{2h} & -\frac{aP_2(Q_1-\delta P_1\lambda_1-P_1\lambda_4)}{2h} & -\frac{aP_2(\delta\epsilon_5\lambda_1-\lambda_2)}{2h} & -\frac{aP_2(-Q_2+\delta P_2\lambda_1-P_1\lambda_4)}{2h} & -\frac{aP_2(\delta\epsilon_2\lambda_1-\lambda_3)}{2h} \\
\frac{3aP_1\lambda_4}{2h} & \frac{aP_1(Q_1-\delta P_1\lambda_1-P_2\lambda_4)}{2h} & \frac{aP_1(\delta\epsilon_5\lambda_1-\lambda_2)}{2h} & \frac{aP_1(-Q_2+\delta P_2\lambda_1-P_1\lambda_4)}{2h} & \frac{aP_1(\delta\epsilon_2\lambda_1-\lambda_3)}{2h} \\
-\frac{a(1+Q_1^2+Q_2^2)P_1}{2h} & \frac{a(1+Q_1^2+Q_2^2)\delta\epsilon_5}{8h} & 0 & \frac{a(1+Q_1^2+Q_2^2)(1-\delta P_2^2)}{4h} & 0 \\
-\frac{a(1+Q_1^2+Q_2^2)P_2}{2h} & \frac{a(1+Q_1^2+Q_2^2)(1-\delta P_1^2)}{4h} & 0 & \frac{a(1+Q_1^2+Q_2^2)\delta\epsilon_5}{8h} & 0
\end{bmatrix} \tag{70}
$$

$$
M_S = \begin{bmatrix}
-\frac{2a^2(\epsilon_1-1)}{h} & 0 & 0 & 0 & 0 \\
0 & \frac{\delta(\delta\epsilon_1-1)(a\mu+h^2)P_1}{2h\mu} & -\frac{\delta(\delta\epsilon_1-1)a\epsilon_5\mu}{4h\mu} & -\frac{\delta(\delta\epsilon_1-1)(a\mu+h^2)P_2}{2h\mu} & \frac{\delta(\delta\epsilon_1-1)a\epsilon_2\mu}{2h\mu} \\
\frac{a^2\mu(\epsilon_1+2h^2)P_1}{2h\mu} & -\frac{a\delta(b\mu-h^2)}{4h\mu} & -\frac{a^2\mu P_1(\epsilon_1-1)}{4h\mu} & -\frac{a(2\delta\mu(a\epsilon_1+b\epsilon_3)+2h^2(\delta\epsilon_4-1))}{4h\mu} & -\frac{a\delta\mu P_2(a(1-\epsilon_1)+b(1-\epsilon_5))}{4h\mu} \\
\frac{a(a\mu(\epsilon_1-1)-2h^2)P_2}{2h\mu} & \frac{a(-2\delta\mu(a\epsilon_1+b\epsilon_4)-2h^2(\delta\epsilon_3+b)+2a^2\mu)}{2h\mu} & \frac{a\delta\mu P_2(a(\epsilon_1-1)-b(\epsilon_2-1))}{2h\mu} & \frac{a^2(h^2-b\mu)\epsilon_5}{4h\mu} & \frac{a\delta\mu P_1(a(\epsilon_1-1)+b(P_2^2+\epsilon))}{4\mu} \\
0 & 0 & 0 & 0 & 0 \\
0 & 0 & 0 & 0 & 0
\end{bmatrix} \tag{71}
$$

Where,

$$
\epsilon_1 = P_1^2 + P_2^2 \qquad \epsilon_2 = P_1^2 - P_2^2 \qquad \epsilon_3 = P_1^2 - 1 \qquad \epsilon_4 = P_2^2 - 1 \qquad \epsilon_5 = 2P_1P_2
$$

$$
\delta = \frac{a}{a+b} \qquad \lambda_1 = P_1Q_1 + P_2Q_2 \quad \lambda_2 = P_1Q_2 + P_2Q_1 \quad \lambda_3 = P_1Q_1 - P_2Q_2 \quad \lambda_4 = P_1Q_2 - P_2Q_1
$$

4. Numerical Verification

The configuration of a modeled spacecraft for numerical verification is set as 4 mN on the maximum thrust power, and 500 kg on spacecraft mass. Numerical verification compare the analytical method and numerical integration method with some thrust maneuvering models and initial osculating orbit elements.

4.1. Comparison with Benefit of Accuracy on 1 Revolution

The first verification model is randomly maneuvering thrust pattern for one revolution as shown in Figure.1. The black line is the virtual thrust pattern as actual maneuvering up to 10^{th} order Fourier series. The red dashed line represents lower-frequency maneuvering which only takes account of ETFCs. The Figure shows that the red dashed line follows a trend of the black line. Nevertheless, it is obvious that the both forms of detailed thrust are relatively different. The initial osculating eccentricity and inclination is set as considerably low as shown in Table.1. Other osculating orbit elements are set as insignificant numbers. To observe this comparison easily, the number of revolutions is set bound to an one revolution.

Table 1. Testing Initial Condition 1

a	e	i	Ω	ω	M
6771 km	0.001	0.001 deg	45.0 deg	22.5 deg	0 deg

Figure 1 shows a comparison of the results of the two methods. It can be seen that it is possible to calculate the osculating orbital element after one revolution while ignoring short-term fluctuation in the analytical method. Furthermore, note that the computational time with the analytical one is considerably reduced. Figure 2 shows the accuracy of the new analytical method by comparison with previous analytical methods, which uses the variational equations with Keplerian. In the previous method, long-term fluctuations could not be followed. Since the value of eccentricity is negative, it will result in more errors in the second iteration. In contrast, the new analytical solution can follow the long-term variation as well as in the result of the osculating equinoctial elements as shown in Figure 1.

4.2. Many-Revolution cases

Next, many-revolution case are analyzed under the same conditions as the previous one. The result on osculating equinoctial elements are shown in Figure 4. The analytical method can follow the secular variation. The analytical solution Q_2 gradually differs from the exact one. Since the value of Q_2 itself is relatively small, it does not significantly affect other elements. Therefore, in order to prevent the order of values from being largely different from each other, it is necessary to devise in numerical calculations such as nondimensionalization. In Figure 5, it shows that there is a significant validity of the analytical results.

Subsequently, the case of some other controls are also verified. One is to control in the out-of-plane direction and the other is to control thrust in the in-plane direction. By verifying each of them, it was verified whether the specificity of eccentricity and inclination can be avoided.

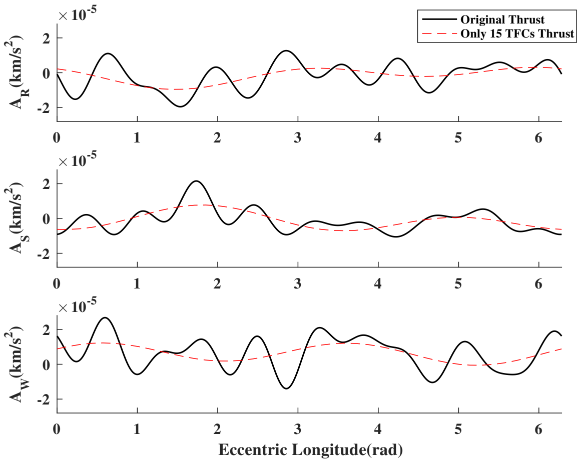

Fig. 1. Thrust acceleration curve of randomly maneuvering pattern: Black line is calculated with randomly generated 10th Fourier Orders. Red dashed line is calculated with only ETFCs (2nd Fourier Orders)

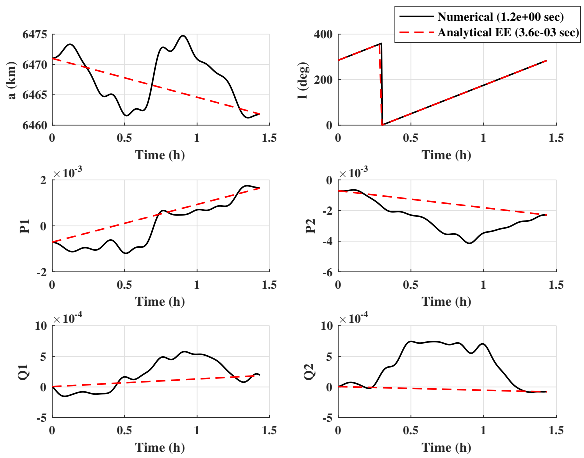

Fig. 2. Comparison with numerical and analytical method on osculating equinoctial elements; Black line shows the numerical propagation method with 10th Fourier Coefficients, and red dashed line shows the analytical integration with only KTFCs. (Testing thrust curve: Figure 1, Initial Condition: Table 1)

4.2.1. Out-of-Plane Control

It is assumed that the control is only performed stepwise in the out-of-plane direction A_W as shown in Figure 6. In this case, the maneuvering interval is for 90deg.

The initial conditions are tested on two cases. The first one is the low-eccentricity case (Table 2), and the other is high-eccentricity case (Table 3).

Table 2. Testing Initial Condition 2

a	e	i	Ω	ω	M
6771 km	0.0001	0.5 deg	45.0 deg	22.5 deg	0 deg

Table 3. Testing Initial Condition 3

a	e	i	Ω	ω	M
6771 km	0.3	0.5 deg	45.0 deg	22.5 deg	0 deg

In the first case of initial condition, both the osculating elements are significantly matched. it is notable that the secular fluctuations of inclination are close to zero and increase again. This says that the orbital plane is crossing over the reference

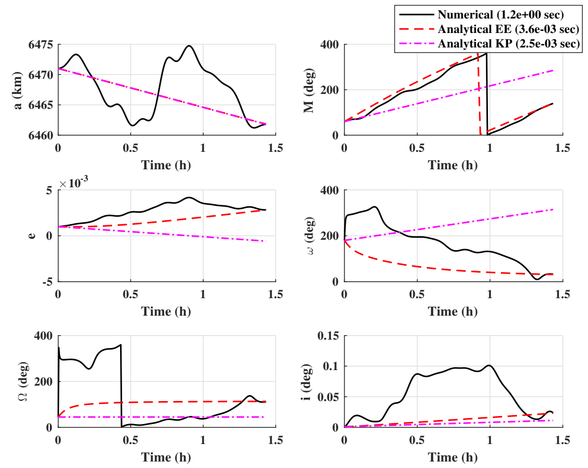

Fig. 3. Comparison on osculating Keplerian elements. Black line and Red dashed line are transformed from equinoctial elements (Figure 2). Magenta dash-dotted line is calculated by original TFCs theory with only KTFCs. (Testing thrust curve: Figure 1. Initial Condition: Table 1)

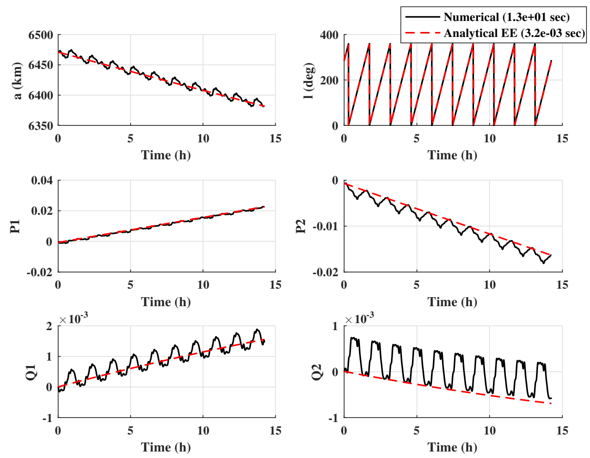

Fig. 4. Comparison on osculating equinoctial elements with 10 revolutions. (Testing thrust curve: Figure 1, Initial Condition: Table 1)

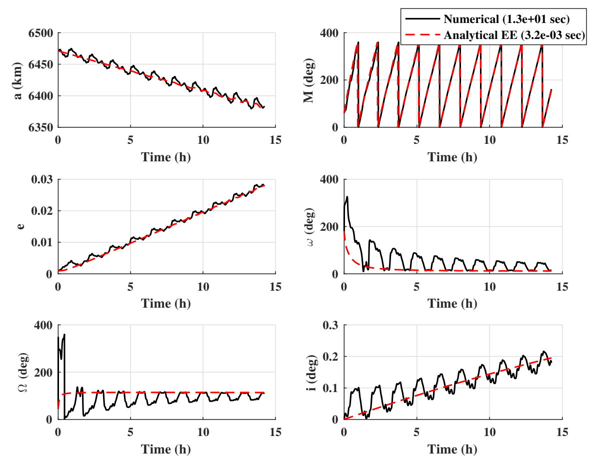

Fig. 5. Comparison on osculating Keplerian elements with 10 revolutions. (Testing thrust curve: Figure 1), Initial Condition:Table 1)

plane. Such dynamical behavior can not be calculated with a original TFCs method due to the indefinite of the line of ascending node.

In the second case of initial condition, the analytical solutions are obviously different from exact solutions. This is caused by the non-negligible product of both the deviation of radius and differential elements ⟨r'ǣ$'$⟩ as shown in Eq.61. This fact proves that this new analytical solutions are can not be use in high-eccentricity case.

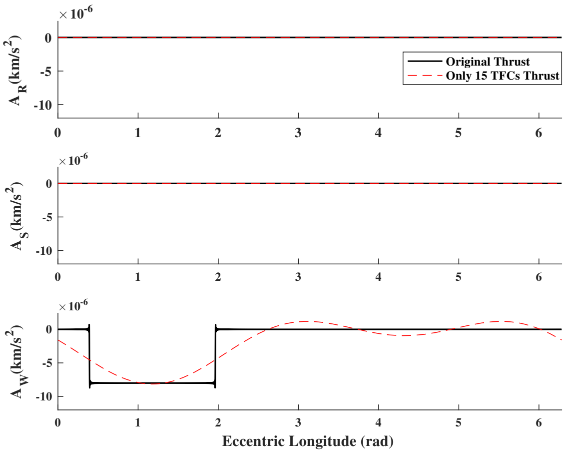

Fig. 6. Only maneuvering normal direction: Black line is calculated with randomly generated 1000th Fourier Orders. Dashed Red line is depicted with only ETFCs (2nd Fourier Orders). To change inclination angle, normal direction is only maneuvered.

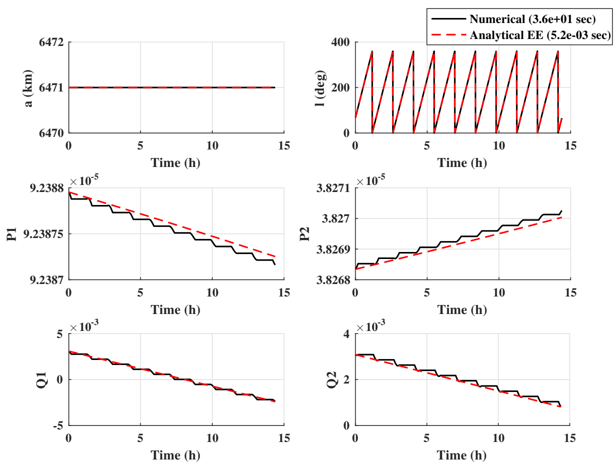

Fig. 7. Comparison on osculating equinoctial elements with 10 revolutions. (Testing thrust curve: Figure 6 Initial Condition: Table 2)

4.2.2. In-Plane Control

The initial condition of this case is Table 4. To see the avoiding the singularity of eccentricity, in other words, the uncertainty of priapsis. It is assumed that control is only performed stepwise in the in-plane direction A_S as shown in Figure 11. This thrust curve performs acceleration at apoapsis to raise periapsis and decelerate at periapsis to descendens apasis. Seeing the Figure 13, After eccentricity is close to zero, it raises to become elliptic orbit again. Furthermore, argument of periapsis turnovers 180 degrees. This result says that the south-east maneuver can be calculated with the new analytical solution while avoiding the singularity of eccentricity.

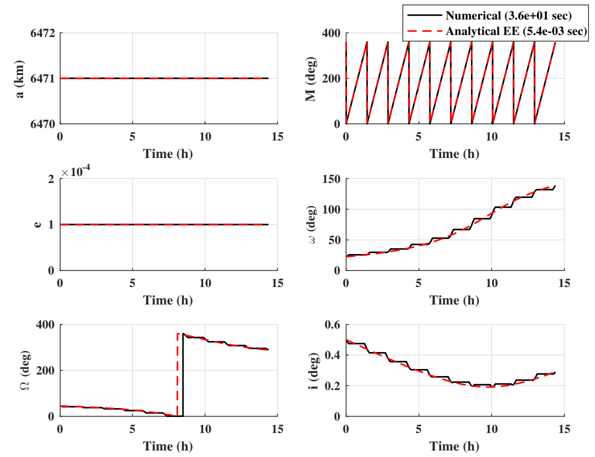

Fig. 8. Comparison on osculating Keplerian elements with 10 revolutions.(Testing thrust curve: Figure 6 Initial Condition: Table 2)

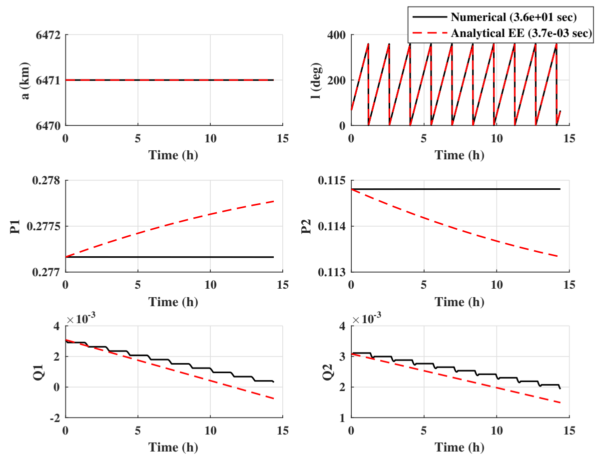

Fig. 9. Comparison on osculating equinoctial elements with 10 revolutions. (Testing thrust curve: Figure 6 Initial Condition: Table 3)

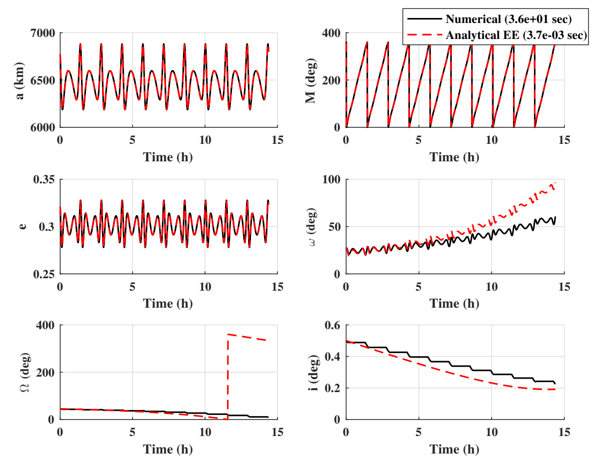

Fig. 10. Comparison on osculating Keplerian elements with 10 revolutions. (Testing thrust curve: Figure 6 Initial Condition: Table 3)

Table 4. Testing Initial Condition 4

a	e	i	Ω	ω	M
6771 km	0.03	10 deg	45.0 deg	22.5 deg	0 deg

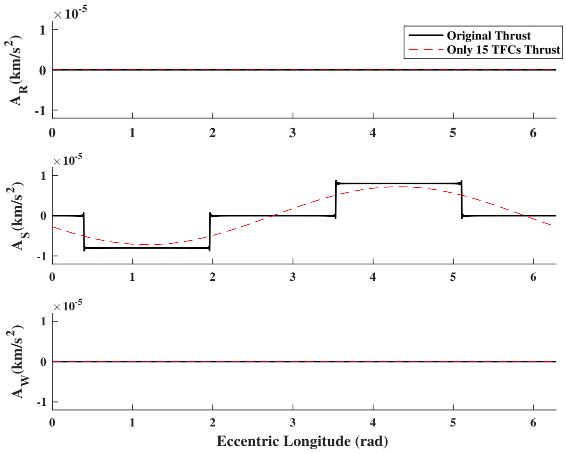

Fig. 11. Only maneuvering circumferential direction: Black line is calculated with randomly generated 10^{th} Fourier orders. Dashed Red line is depicted with only ETFCs (2nd Fourier Orders)

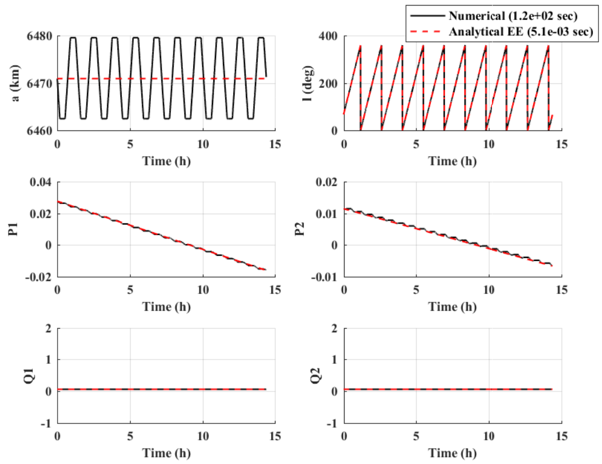

Fig. 12. Comparison on osculating equinoctial elements with 10 revolutions. (Testing thrust curve: Figure 11 Initial Condition: Table 4)

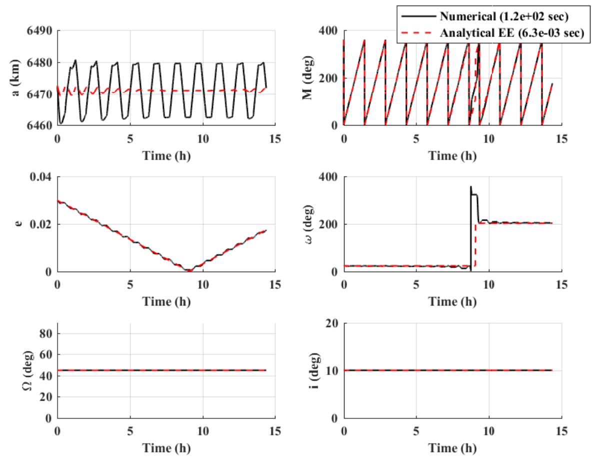

Fig. 13. Comparison on osculating Keplerian elements with 10 revolutions. (Testing thrust curve: Figure 11 Initial Condition: Table 4)

5. Conclusion

The analytical solutions, which use equinoctial elements and are averaged with TFCs theory, was found under the assumptions of low-eccentricity. The solutions can be used for the terminal sequence of approaching GEO, and station-keeping operation for a geostationary satellite. The method developed is not applicable for high-eccentricity due to the assumption of low-eccentricity while developing process; however, an analytical solutions with the original TFCs theory can solve the high-eccentricity case. When these methods are combined, designing more general transfer could be realized with flexible thrust direction. The KTFCs and ETFCs can be inputted on a multi-objective optimizer as a design parameter. The resulting thrust history could be a good initial estimate solution for a more detailed trajectory design.

References

1) J.A. Kechichian. Low-Thrust Eccentricity-Constrained Orbit Raising. *Journal of Spacecraft and Rockets*, 35 1998. pp327–335.
2) J.A. Kechichian. Orbit Raising with Low-Thrust Tangential Acceleration in Presence of Earth Shadow. *Journal of Spacecraft and Rockets*, 35 1998. pp516–525.
3) F.Zuiani and M.Vasile. Extention of Finite Perturbative Elements For Multi-Revolution, Low-Thrust Transfer Optimization. In *63rd International Astronautical Congress.* Naples, Italy, 43, Oct 2012, pp.661–673,
4) J.S. Hudson and D.J. Scheeres. Reduction of Low-Thrust Continuous Controls for Trajectory Dynamics. *Journal of Guidance, Control, and Dynamics*, 32(3) May 2009 pp.780–787
5) R.H. Battin. *An Introduction to the Mathmatics and Methods of Astrodynamics*. AIAA Education Series, 1987.
6) Oliver Montenbruck and Eberhard Gill. *Satellite Orbits*. Springer-Verlag Berlin, 2000.
7) J.M.A. Danby. *Fundamentals of Celestial Mechanics*. Willmann-Bell, Richmond, VA, 2 edition, 2003.